SCIENTIFIC REPORTS

OPEN

SUBJECT AREAS:
TECHNIQUES AND INSTRUMENTATION
GENE DELIVERY

Received
11 October 2013

Accepted
30 April 2014

Published
29 May 2014

Correspondence and requests for materials should be addressed to S.K.M. (smohanty@uta.edu)

Crystalline magnetic carbon nanoparticle assisted photothermal delivery into cells using CW near-infrared laser beam

Ling Gu[1], Ali R. Koymen[2] & Samarendra K. Mohanty[1]

[1]Biophysics and Physiology Lab, Department of Physics, University of Texas at Arlington, Arlington, TX 76019, [2]Department of Physics, University of Texas at Arlington, Arlington, TX 76019.

Efficient and targeted delivery of impermeable exogenous material such as small molecules, proteins, and plasmids into cells in culture as well as *in vivo* is of great importance for drug, vaccine and gene delivery for different therapeutic strategies. Though advent of optoporation by ultrafast laser microbeam has allowed spatial targeting in cells, the requirement of high peak power to create holes on the cell membrane is not practical and also challenging *in vivo*. Here, we report development and use of uniquely non-reactive crystalline magnetic carbon nanoparticles (CMCNPs) for photothermal delivery (PTD) of impermeable dyes and plasmids encoding light-sensitive proteins into cells using low power continuous wave near-infrared (NIR) laser beam. Further, we utilized the magnetic nature of these CMCNPs to localize them in desired region by external magnetic field, thus minimizing the required number of nanoparticles. We discovered that irradiation of the CMCNPs near the desired cell(s) with NIR laser beam leads to temperature rise that not only stretch the cell-membrane to ease delivery, it also creates fluid flow to allow mobilization of exogenous substances to the delivery. Due to significant absorption properties of the CMCNPs in the NIR therapeutic window, PTD under *in vivo* condition is highly possible.

The introduction of foreign DNA[1], short-interfering RNA[2], proteins[3], drugs and other small molecules into living cells, organs and whole organisms is essential for a variety of applications in genetics, cell and developmental biology, vaccination[4], gene therapy[5,6] and other therapeutic strategies. DNA delivery for gene therapy (while in its infancy) is of primary importance to the future treatment of certain diseases by allowing correction to be made to the defective genes. Further, the transfection of plasmids encoding fluorescent proteins[7] are routinely used to visualize cellular and sub-cellular structures and also to study various functional aspects of cell and developmental biology[8]. This has led to several important discoveries in biology and medicine. Recent development of optogenetics has further highlighted the value of gene molecule delivery into cells[9–12]. By targeted delivery of genes coded for light-sensitive opsins, selected groups of excitable cells (neuronal, muscle, cardiac, etc) can be specifically stimulated or silenced with high temporal precision by low-power light[9,10]. This hybrid optogenetics[11] approach has heavily impacted neuroscience by allowing dissection of neuronal circuitry, which may prove valuable in the treatment of several neurological disorders. However, the complexity of existing gene delivery systems poses a major obstacle[6] in translating gene therapy methods into clinical practice. The primary method of gene delivery employs viral transfection[12–14], which has high transduction efficiency and persistent gene expression. However, use of viruses can lead to unexpected inflammatory responses, immunological reactions, improper gene integration and limit the size of plasmids that can be packaged and delivered[6,15]. Further, viral methods cannot be applied to the delivery of proteins, impermeable drugs, or small molecules, which are required for vaccination and treatment of cancer. Therefore, there have been significant efforts in developing alternative, non-viral methods such as physical (microinjection[16], electroporation[17,18], ultrasound[19] etc) and chemically-mediated (e.g. Dextran, liposomes[20], and biodegradable polymer[21]) methods. These methods suffer from one or more drawbacks, such as invasiveness, reduced efficiency, lack of spatially-targeted delivery and/or having several deleterious effects on transfected cells[17]. For example, though gene-delivery based on physical methods using naked plasmid DNA is considered to be safe due to ease of handling and lack of the immune response (compared with viral vectors methods), physical energy required for in-vivo delivery into large animals

using classical physical methods, namely electroporation or photo-mechanical waves, can cause physical and functional damage to the tissue. Similarly, it is difficult to spatially control the region of gene expression using virus vectors or chemically-mediated (liposomes and polymer nanoparticles) methods. For gene therapy applications, site-specific gene delivery is particularly important in order to avoid gene expression in non-targeted sites.

Contrary to other physical methods, use of a tightly-focused pulsed laser beam, the membranes of targeted cells in a minute region can be perforated (optoporated) in a minimally-invasive manner, allowing exogenous molecules to enter the cell. Over the last two decades, laser-assisted perforation has been applied to inject macromolecular substances into single plant and animal cells in a non-contact and non-invasive manner. Initially, lasers in UV[22] and visible spectral range (such as 488 nm[23,24]) were employed for optoporation. However, UV-Visible light has increased potential of damage to cellular organelles as well as to the foreign molecules (such as DNA and proteins) being transferred into the cells. Further, since significant scattering and absorption of UV-visible light occurs during propagation in tissue, it is difficult to use these wavelengths for deeper penetration into *in vivo* tissues or organs. Recently, lasers in the near infrared region (NIR, 700–1000 nm), referred to as the 'biological window', have received increasing attention because of significantly lower optical loss due to absorption and scattering by cellular component in this range[25–28]. However, high peak intensity of ultrafast (nanosecond[25], picoseconds[28] and femtosecond[29,30]) laser beam is required to microinject exogenous materials into the targeted cells. Though these pulsed lasers are suitable for single cell in-vitro microinjection, difficulties arise for in-vivo delivery of molecules into 3D tissues due to several reasons. The first reason is that the efficiency and throughput for *in-vivo* delivery is low while using this method, as it requires high peak intensity of laser beam which needs to be scanned to deliver molecules into a region of interest. Secondly, the laser beam profile (focusing) and pulse will be distorted during propagation inside tissue, thus losing the required intensity to cause in-depth perforation. Increasing the laser energy further can cause severe damage to non-targeted cells and tissues before ever reaching the targeted tissues. The third reason that inhibits scanning femtosecond (fs) laser beam the usage for *in-vivo* delivery is the inherent difficulty of clinical implementation. The instruments' bulk and complexity represent serious operational difficulties. Therefore, application of fs laser based poration has been mostly limited to *in-vitro* and monolayer cell-culture.

Therefore, we set ourselves the goal of enhancing the interaction of light with cell membrane by use of photothermal agents so that a continuous wave (CW) laser beam can be used for targeted delivery. Photothermal agents are usually developed to have strong absorption around a selected wavelength so as to avoid the competition of light absorption by native tissue chromophores. This enhances the effectiveness of heat deposition on targeted cells and reduces non-targeted injury to adjacent tissues. In recent years, nanotechnology has become one of the most exciting forefront fields in cancer diagnosis and therapeutics to enable drug delivery[31–33], thermal therapy[34,35] and detection of circulating cancer cells[36,37]. Carbon nanomaterials such as carbon nanotubes[38–40] and gold nanostructures including nanoparticles[31,32,41], nanorods[42,43], nanoshells[44,45] and nanocages[46] are most commonly used in drug delivery, tumor cell imaging and photothermal therapy due to their strong absorption in NIR field. Recently, we developed[47] magnetic carbon nanoparticles (MCNPs) and used hybrid field (localization by magnetic field and irradiation with NIR CW laser) to efficiently cause photothermal destruction of cancer cells. Here, our approach utilizes crystalline magnetic carbon nanoparticles (CMCNPs) and magnetic field as well as NIR CW laser beam to realize photothermal delivery (PTD) of impermeable dyes and plasmids into targeted mammalian cells. The strong absorption of these CMCNPs in NIR region allowed efficient conversion of NIR light to heat and the magnetic properties allowed their effective localization in target areas by an external magnetic field. Our study suggests that CMCNP based and magnetic-filed assisted photothermal delivery is a viable approach to remotely guide drug and gene delivery.

Results

Unlike the ultrafast fs laser microbeam, a CW laser beam in NIR does not have enough intensity to perforate cell membranes directly. However, by use of suitable nano agents, photothermal effects can be enhanced. In Fig. 1(a), we show the principle of carbon nanoparticles mediated photothermal delivery (PTD) using CW NIR laser beam. The local temperature rise is sufficient to stretch the cell membrane, and thus, microinject exogenous molecules into the cells exposed to both CW laser beam and photothermal agents (Fig. 1a). Furthermore, the rise in the temperature leads to convection in the extra-cellular media, which drives the molecules-to-be-injected towards the injection site, thus enhancing the probability of delivering. Our approach utilizes a hybrid-field application for efficient photothermal delivery using crystalline magnetic carbon nanoparticles (CMCNPs) with a strong absorption in the NIR (700–1000 nm) region. For synthesis of the CMCNPs, electric plasma discharge was generated between two iron electrodes in the cavitation field of an ultrasonic horn in liquid benzene (see methods for details). Suppl. Fig. 1 shows the schematic setup for synthesis of the CMCNPs. In this method, the contrast in temperature rise of CMCNP-localized cells vs. surrounding cells is significant enough to allow site-specific delivery of exogenous molecules. It may be noted that positioning of the NIR CW laser beam can be controlled so as to achieve targeted delivery into cell(s) of interest in-vitro. However, it is difficult to achieve so at large depths and therefore either physical or chemical functionalization methods can be utilized to enhance the targeted delivery.

Here, we utilized the magnetic nature of the CMCNPs to allow application of external DC magnetic field (gold-coated Neodymium Iron Boron magnet) to localize them in targeted regions of monolayer of cells as shown in the schematic (Fig. 1b). The size of the CMCNPs, prepared at 4.1 kV, was found to range from 5–20 nm (TEM image, Suppl Fig. 2a, b) which has significance in translating the technology for future in-vivo application as it will allow easy excretion by reticuloendothelial system. Notably, as shown in the high resolution TEM image (Fig. 1c and Suppl. Fig. 2b) the CMCNPs are highly crystalline in nature and were found not to dissolve in concentrated (70%) HNO_3 acid, even after 10 min of heating using a Bunsen burner. This unique property led us to believe that the CMCNPs are very non-reactive and stable which is important for minimal cytotoxicity. To evaluate the dark cytotoxicity, we incubated the CMCNPs with PC3 cells in 5% CO_2 and humidified atmosphere for 3 hours before experiment. MTT assay was utilized to evaluate the cytotoxicity (without laser irradiation) with different concentration of CMCNPs and incubation times. While a higher concentration of nanoparticles (250 μg/ml) decreased the viability of cells ($p < 0.05$), lower concentrations (2.5 μg/ml and 25 μg/ml) of CMCNPs incubated for as long as 6 hr did not significantly decrease the viability of the PC3 cells (data not shown). Interestingly, the selected area electron diffraction (SAED) image of these CMCNPs (Suppl. Fig. 2c) showed that these crystalline CNPs have unique lattice spacing, not matching to that of lattice spacing of known isoforms of carbon, namely graphite and diamond etc (Suppl. Table 1). The absorption spectrum of the CMCNPs in near-infrared spectrum is shown in Suppl. Fig. 2d. Higher D-band (~1300 nm) in the Raman spectrum (Suppl. Fig. 2e) as compared to the G-band (~1600 nm) showed that structure of these CMCNPs may have some form of diamond-like-carbon.

In addition to unique crystalline properties, these CMCNPs were found to be magnetic as confirmed by measurements of specific

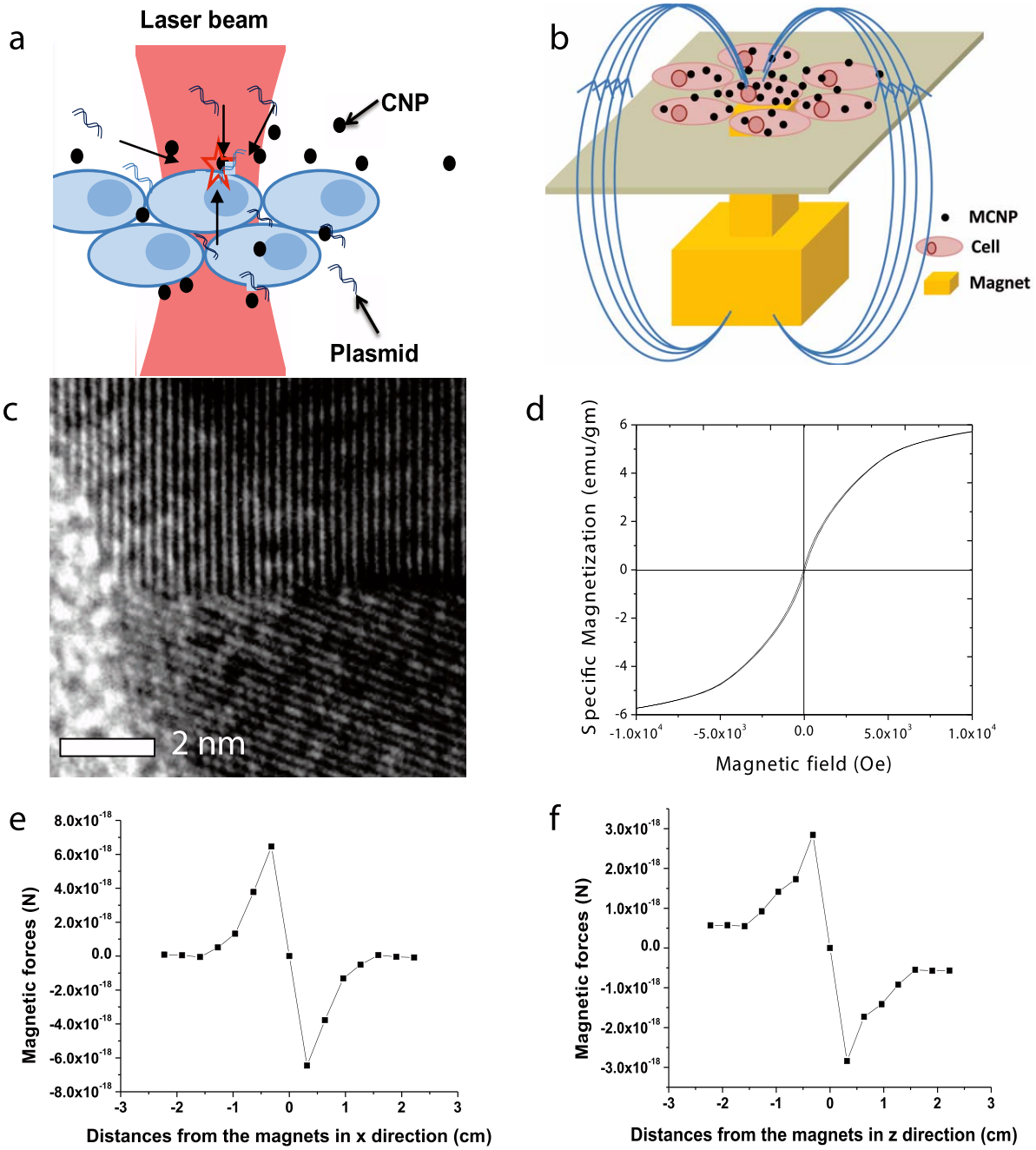

Figure 1 | (a) Principle of carbon nanoparticles mediated Photothermal delivery using CW laser beam. (b) Schematic of external magnetic field assisted localization of magnetic carbon nanoparticles. (c) HRTEM image of crystalline magnetic carbon nanoparticles (CMCNPs) prepared at 4.1 kV, (d) Specific magnetization measured at room temperature with a VSM. Magnetic forces estimated on the CMCNPs in (e) transverse (X) and (f) axial (Z) directions.

magnetization using vibrating sample magnetometer (VSM). Magnetic measurements showed that the MCNP powder sample is ferromagnetic with a low ratio of remnant to saturation magnetization (Fig. 1d). The origin of magnetic properties owes to the fact that during the synthesis process, Fe-electrodes erode and 1–2% of Fe gets embedded into the carbon matrix (formed from benzene) of CMCNPs. The Fe-content is confirmed by the energy dispersive X-ray analysis of these CMCNPs (Suppl. Fig. 2f). It may be noted that with different electric field (voltage applied between the electrodes) % of iron content in the CMCNPs can be controlled. In order to evaluate effect of external DC magnetic field on the CMCNPs, the magnetic force on the CMCNPs was estimated using the measured saturation magnetization (Fig. 1d) value. For the force estimations the magnetic field of the external magnet was measured by a Gauss meter utilizing the Hall-effect. The magnetic force $F = -\nabla\varphi$ (where the scalar potential $\phi = -\mu.B$) was estimated from the gradient of magnetic field (∇B) generated by the specific external magnet to-be-used in the PTD experiments. Using graph for specific magnetization for CMCNP (Fig. 1d), we obtain $\chi = 1.9386 \times 10^{-4}$ emu/g Oe, which leads to $\mu = 1.0002$ (see methods for details). In Fig. 1e, we show the theoretically estimated magnetic force on the CMCNPs in transverse (X or Y) direction. Fig. 1f shows the force on the CMCNPs in axial (Z) direction. The forces were found to increase significantly within ± 2 mm and then decrease. The maximum force was estimated to be 6.5×10^{-18} N in transverse directions and 2.8×10^{-18} N in axial direction. The restoring nature of the magnetic force (as shown in

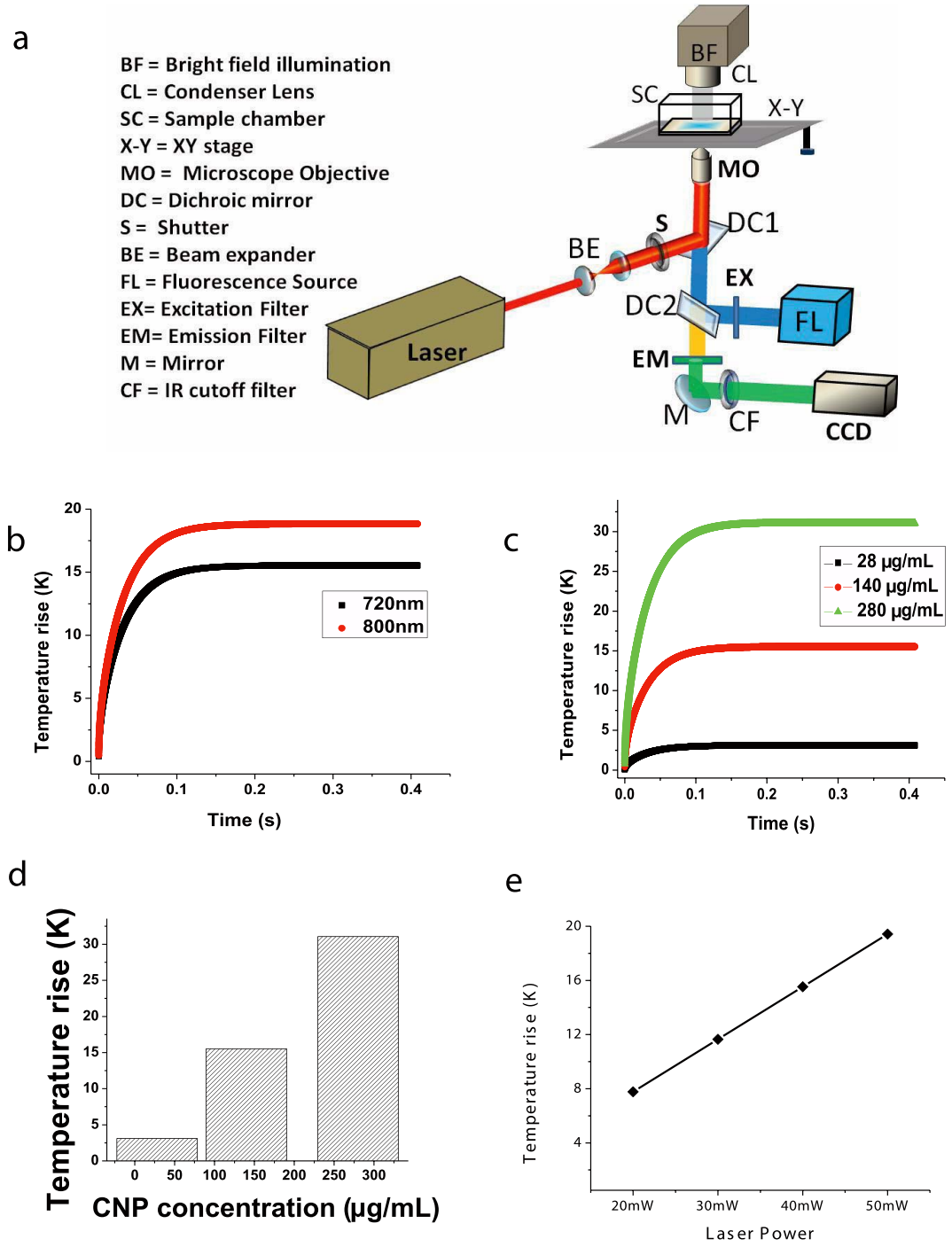

Figure 2 | (a) Schematic of the experimental setup for irradiation of CMCNP-cells using near-infrared (NIR) laser beam (external magnet not shown). Kinetics of theoretically estimated temperature rise in the focal volume of laser beam for (b) two different NIR wavelengths and (c) three different CMCNP concentrations. (d) Estimated saturated temperature rise at focal volume irradiated with 720 nm and 40 mW cw laser beam, as a function of CMCNP concentration. (e) Variation of temperature rise with laser beam power.

Fig. 1e & f) towards center assisted in localizing the CMCNPs near the targeted PTD site by application of an external magnetic field.

In Fig. 2a, we show the schematic of the experimental setup for irradiation of CMCNP-cells using near-infrared (NIR) laser beam (external magnet not shown). Details about the set up are described in methods. CMCNPs were found to be accumulated on targeted cells with application of external DC magnetic field. Analysis of microscopic images of CMCNPs showed that the concentration increased with increase in duration of the external magnetic field application. Since heat generated by photothermal means is dependent on concentration of the photothermal agent in the laser irradiation volume, application of external magnetic field reduced the overall dose of CMCNPs used for PTD by maximizing the concentration of the CMCNPs at the targeted area. In order to find the optimal time (for specific external magnetic field) required to concentrate necessary amounts of CMCNPs to generate sufficient heat at an allowed laser irradiation dose, numerical simulation of temperature rise by CMCNP-mediated photothermal means was carried out (details in method). The absorbance (A) of CMCNPs in the NIR region was measured using a spectrophotometer (Perkin Elmer),

which showed significant absorption in the NIR region. The absorbance at 800 nm and 720 nm was measured to be 0.115 and 0.095 respectively. Using Beer–Lambert's law ($A = -\log I/I_0 = \varepsilon cl$, A: absorbance; ε: extinction coefficient, c: concentration of CMCNP; *l*: path length), the extinction coefficient at 800 nm and 720 nm was estimated to be 4.11 $ml.mg^{-1}cm^{-1}$ and 3.39 $ml.mg^{-1}cm^{-1}$ respectively.

For theoretical estimation of temperature rise, the absorption of the laser energy directly by the cells was neglected due to their extremely low absorption cross section in NIR, as compared to that of CMCNPs. The temperature of media surrounding CNPs was found to depend on laser irradiation time, the concentration of CMCNPs, the wavelength and power of the laser beam. As shown in Fig. 2b, the temperature rise was nonlinearly dependent on the time for irradiation. Fig. 2b shows the kinetics of estimated temperature rise in the immediate vicinity of the heated CMCNPs (concentration: 140 μg/mL) for two different NIR laser wavelengths having same laser power (40 mW). As shown in Fig. 2b, the temperature of cell membranes in immediate vicinity of CMCNPs will increase and saturate within 0.2 s. The temperature increased 15.5 K when irradiated by laser beam with wavelength of 720 nm as compared to 18.8 K for 800 nm. Larger saturated temperature in case of 800 nm can be attributed to its higher extinction coefficient as compared to 720 nm. In Fig. 2c, we show the kinetics of theoretically estimated temperature rise in the focal volume of laser beam (720 nm, laser power: 40 mW) for three different CMCNP concentrations. The estimated saturated temperature rise at focal volume was found to increase with CMCNP concentration (Fig. 2d). The spatial distribution of temperature around the CMCNP (after 0.4 s irradiation) showed that the temperature decreases with increasing distance from the CMCNP center (Suppl. Fig. 3a). Further, the saturated peak temperature rise was found to increase linearly with the power of the laser beam (Suppl. Fig. 3b and Fig. 2e). The localized temperature rise on the cell membrane by the photothermal effect of CMCNPs will lead to localized membrane stretching and thus generate nano holes in the plasma membranes. However, large temperature rise can cause loss of cell viability. Therefore, optimized laser intensity and concentration of CMCNPs has to be applied for causing temperature rise necessary to induce successful PTD.

Using the optimized parameters for selectively concentrating CMCNPs and efficiently generating heat, we carried out targeted photothermal delivery of exogenous impermeable dyes and plasmids into different mammalian cells. CMCNPs (28 μg/mL) were incubated with variety of cancer cells (human prostate cancer cells and human fibroblast sarcoma cells). External DC magnetic field (by Gold-coated Neodymium Iron Boron magnet) was applied for 2 hr to accumulate CMCNPs in the area of interest before experiments. The concentration of CMCNPs in the petridish region near the center of the external gold-coated magnet was found to be much higher than that under no or weaker magnetic field (5 mm away from magnets). The increased accumulation of CMCNPs is advantageous in lowering the dose of the CW NIR laser beam and/or the incubated dose of CMCNPs for achieving required temperature rise in the targeted cells (see Fig. 2c). While scanning electron microscopy showed that few CMCNPs are attached to the membrane, most of the CMCNPs were in close vicinity. For photothermal poration, a tunable (690–1040 nm) CW Ti: Sapphire laser beam was weakly focused on to the cell monolayer under an inverted fluorescence microscope (Fig. 2a). For validation experiments, HT1080 cells in monolayer were incubated with impermeable fluorescent dye propidium iodide (PI). Targeted cell (Fig. 3a) incubated with CMCNPs and PI, was micro-irradiated with the CW NIR laser beam (720 nm, 40 mW) and PTD of PI was monitored using time-lapse fluorescence imaging. Fig. 3b shows the PI fluorescence before laser irradiation. In Fig. 3c, we show the bright field image of cells after 2 second of application of laser beam (marked by white arrow). Interestingly, the temperature rise not only led to visible stretching of the targeted cell membrane (as seen in Suppl. Movie 1), flow of external media was observed (Suppl. Movie 1). A CMCNP was used as a tracer particle and its direction of movement during laser irradiation is marked by black arrow (Fig. 3c) towards the PTD site. Fig. 3d to i shows time-lapse fluorescence images of photothermally-delivered increase in intra-cellular PI. PI was found to stain the nucleus from the site of injection and propagate through the nucleus by diffusion as shown in time lapse series. This confirms the fact that PI is injected via the pore formed by photothermal delivery and other parts of the cell membrane are intact subsequent to laser irradiation. The bright field image of cells 90 seconds after PTD (Fig. 3j) showed no morphological changes (damage) in the targeted cell. While increase in fluorescence intensity clearly demonstrated delivery of PI into targeted cell, movement of tracer CMCNPs towards PTD site indicated that the CW laser based PTD method can enhance the delivery of exogenous molecules into cell by mobilizing them towards the laser irradiation site. In Fig. 3k, we show the relative position (distance from the site of PTD) of the tracer-CMCNP as a function of laser exposure time. The kinetics of increase in intra-cellular PI fluorescence intensity during PTD is shown in Fig. 3(l). The fact that non-irradiated cells (control) did not show increase in PI fluorescence, indicates low dark-cytotoxicity of CMCNPs. Further, it demonstrates ability of PTD for targeted delivery with high spatial resolution.

Next we aimed to examine the efficacy of PTD into other cell types, namely prostate cancer (PC3) cells. In addition to delivery (or poration), we evaluated the viability of the porated cell by exclusion of intracellular calcium stain (calcein). As shown in Fig. 4a to f, 27 s after laser-assisted (720 nm, 25 mW, 3 sec), photothermal poration, PI was observed to be introduced into the targeted cell (Fig. 4b vs e) by the CW NIR laser microbeam. Since the fluorescence intensity of calcein in the porated cell did not change (Fig. 4 c vs d) as compared to control (surrounding) cells, poration without loss of cell-viability was confirmed. Generation of excess heat by the CW NIR laser beam in presence of CMCNPs can induce cell death in addition to PTD. Therefore, in order to determine the optimal laser power for successful photothermal delivery without losing cell viability, we irradiated PC3 cells (stained with both calcein and propidium iodide) using different laser beam powers. Cells showing both calcein and PI fluorescence 3 min after laser irradiation were considered as being successfully-porated. On the other hand, cells which only showed PI fluorescence were considered as less-viable (or dead). With the fixed irradiation of 3 seconds, we found that low power (25 mW) laser beam (720 nm) was able to achieve better photo-thermal delivery (Fig. 4g). In contrast, higher laser beam power or longer irradiation duration induced more cell damage. In order to evaluate the interplay of laser beam power and wavelength on PTD, we evaluated the PTD efficiency at different wavelengths with varied power levels. The percentage of damaged cells decreased with reduced laser beam power from 75.0% at 50 mW to 18.2% at 25 mW for 720 nm ($n = 9–12$) as shown in Fig. 4g. This was also the case (75.0% at 50 mW to 20.0% at 25 mW) for 800 nm. No significant wavelength-dependent PTD was observed for exposure time (or dose) at higher powers. However, for power levels below 50 mW, the poration efficiency was found to be significantly lower for 800 nm as compared to 720 nm. The percentage of cells being porated increased sharply from 25.0% at 50 mW to 36.4% at 25 mW for 720 nm, but slowly from 25.0% at 50 mW to 30.0% with 25 mW laser at 800 nm ($n = 8–12$) as shown in Fig. 4h. This may be attributed to the difference in absorption coefficient of CMCNPs at these wavelengths (absorption at 800 nm being higher than at 720 nm).

At high laser power (e.g. 92 mW), photothermal damage of irradiated cells occurred in presence of CMCNPs (28 μg/ml) even at very low exposure (<0.2 s). Therefore, lower laser power (<25 mW) need to be used for successful PTD. However, lowering the laser

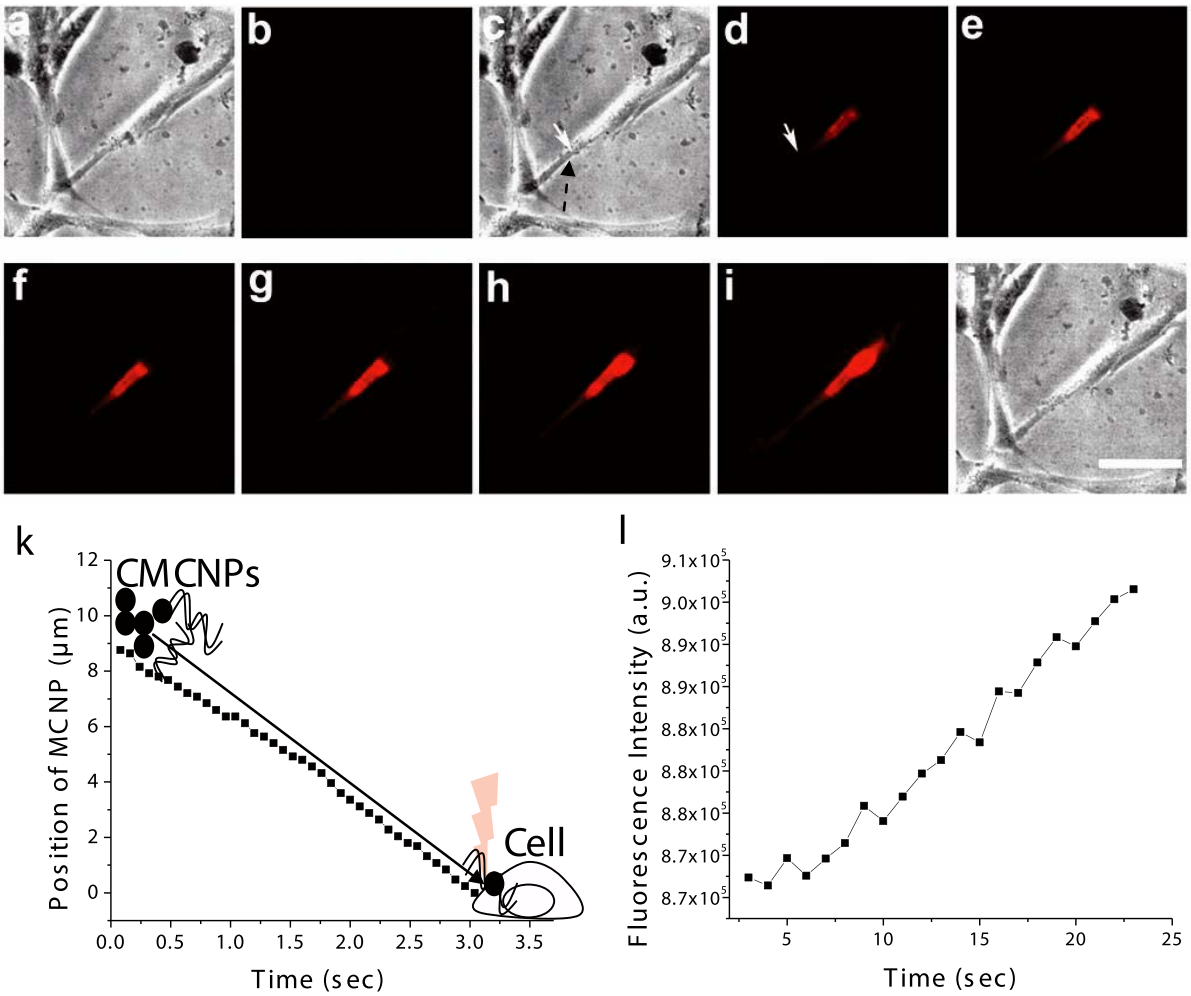

Figure 3 | Kinetics of CMCNP-assisted photothermal delivery (PTD) of impermeable dye (Propidium Iodide, PI) into cells using cw NIR laser beam (720 nm, 40 mW, 3 s exposure). (a) Bright field and (b) fluorescence image of HT1080 cells (incubated with PI) before application of laser beam. (c) Bright field image of cells at 2 second of application of laser beam (marked by white arrow). Black arrow: direction of movement of a tracer-CMCNP towards the PTD site during laser irradiation. (d–i) Time-lapse fluorescence images at 3 s (d), 4 s (e), 5 s (f), 23 s (g), 57 s (h) and 72 s (i) of photothermally-delivered intra-cellular PI. (j) Bright field image of cells 90 s after PTD. Scale bar: 15 μm. (k) Relative position (distance from the site of PTD) of the tracer-CMCNP as a function of laser exposure time. (l) Kinetics of increase in intra-cellular fluorescence intensity during PTD.

power further below 10 mW led to very low efficiency (<5%) of PTD for the concentration of CMCNPs used in this study. Furthermore, we went on to examine the effect of laser exposure duration on photothermal delivery vs. cell damage at lower laser power levels. With exposure up to 3 sec with laser beam power of 25 mW, PTD was found to be associated with no significant (<20%) loss of cell viability (Fig. 4g). However, as shown in Suppl. Fig. 4, we observed formation of microbubbles at reasonable laser power (40 mW) due to accumulated photothermal effect at longer laser exposures (17 sec). Similar effects have been observed earlier by us for higher laser beam power at low exposures. It may be noted that bubble formation can cause damage to the irradiated cell(s) as well as delivery of exogenous molecules to cells surrounding the bubble. While fs laser microbeam lead to cavitation bubbles and stress wave, the CW laser-induced vapor bubbles can be controlled by reducing the exposure time and laser beam power. Thus, bubble-based CMCNP mediated photothermal delivery could also be used for wide-area poration of cells with the cost of damaging cell(s) at the center of the bubble formation site. To ensure that the CW NIR laser beam does not induce photothermal injury of cells in absence of CMCNPs, individual cells were irradiated (without CMCNPs) using CW NIR laser beam (50 mW) for extended exposures (60 sec). Cells stained with calcein (1 μM) for 15 min and propidium iodide (PI, 5 μM) immediately before viewing under fluorescence microscope. While retention of calcein (green fluorescence) indicates living cells, inclusion of PI confirms cells being dead. None of the cells (PC3) without CMCNPs were damaged or porated with PI at this extended NIR laser dose, as determined by PI exclusion assay. Therefore, the CMCNP based photothermal delivery has potential to enable targeted delivery into cells without co-lateral damage. With use of external magnetic field (and/or chemical functionalization) can further the selectivity in targeting cells during in-vivo applications.

In order to evaluate efficacy of CMCNP-mediated PTD for non-invasive delivery of naked DNA to mammalian cells, PC3 cells were incubated with CMCNPs (28 μg/ml) for 2 hr in presence of external magnetic field prior to PTD. ChR2-YFP encoding plasmids (0.5 μg/ml) were added to the extra-cellular medium just before PTD. To transfer the plasmids into the cells, cells in the targeted region of interest were scanned with a CW NIR laser beam (720 nm, 25 mW) with 3 sec exposure per cell. Following PTD, the cells were washed twice with DMEM in order to remove the CMCNPs. 48 hours after photothermal transfection, expression of YFP was detected using epi-fluorescence microscopy. Fig. 5 shows CMCNP-assisted photothermal delivery of ChR2-YFP encoding plasmids into PC3 cells in

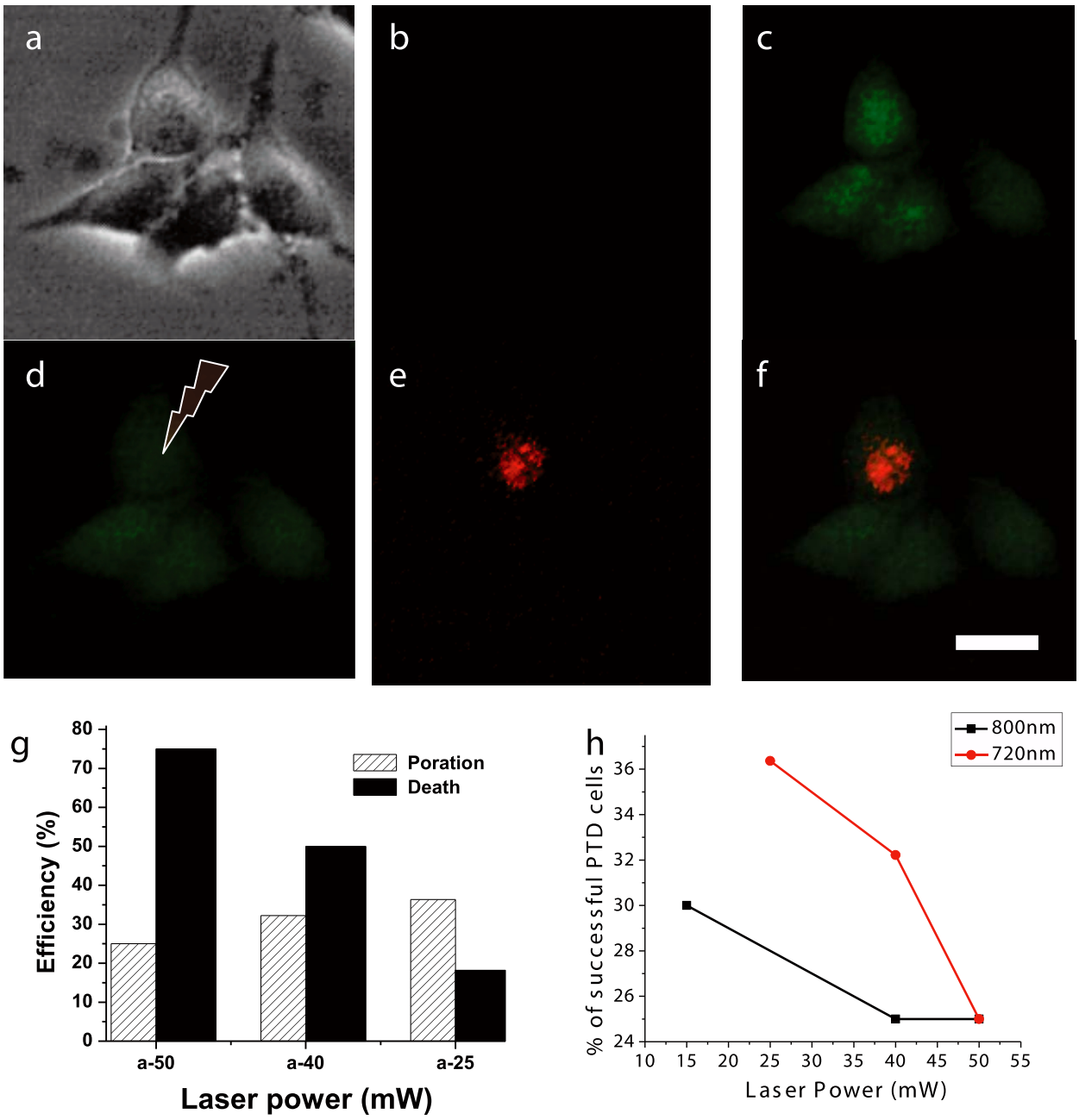

Figure 4 | Efficacy of CMCNP-assisted PTD into prostate cancer (PC3) cells using cw laser beam. Live dead assay: (a) Bright field, (b) propidium iodide (PI) fluorescence and (c) calcein fluorescence before application of laser beam (720 nm, 25 mW, 3 seconds). (d) calcein and (e) PI fluorescence images after 27 s of PTD. (f) Composite image of calcein and propidium iodide fluorescence of targeted PTD-cell (along with surrounding control cells). Scale bar: 10 μm. (g) Percentage of porated vs damaged cells due to PTD (720 nm) at different laser beam powers (n = 9–12). (h) PTD efficiency as a function of power for two different NIR wavelengths (n = 8–12).

two regions of interests using CW NIR laser beam and external magnetic field. Though the transfection efficiency was found to be moderate (~30%) in these regions of PTD, the successful expression of YFP in healthy-looking PC3 cells indicates that magnetic-field assisted CMCNP localization and CW NIR laser beam induced photothermal effect can be used to induce exogenous genes into targeted cells. Incubation with CMCNPs and plasmids only, or plasmids with CW laser irradiation without CMCNPs, did not lead to any YFP expression.

Discussion

We successfully applied hybrid fields (DC magnetic field and CW NIR laser beam) on CMCNPs with unique magnetic and photothermal properties for target-specific delivery of exogenous molecules into various types of mammalian cells. Upon CW NIR laser beam irradiation, the local temperature rise in cell membrane (with CMCNPs) is sufficient to be stretched, thus allowing microinjection of exogenous molecules into the cytoplasm. As a non-viral approach, photothermal delivery can have significant advantages over viral delivery currently used for gene delivery. Though femtosecond laser has been applied earlier for delivery into cells, use of a continuous wave (CW) laser beam with CMCNPs is advantageous as it requires significantly low peak power and thus laser-induced damage to non-targeted cells along the irradiation path can be avoided unlike the case for femtosecond laser beam[48]. Moreover, the application of an external magnetic field to concentrate CMCNPs provides additional

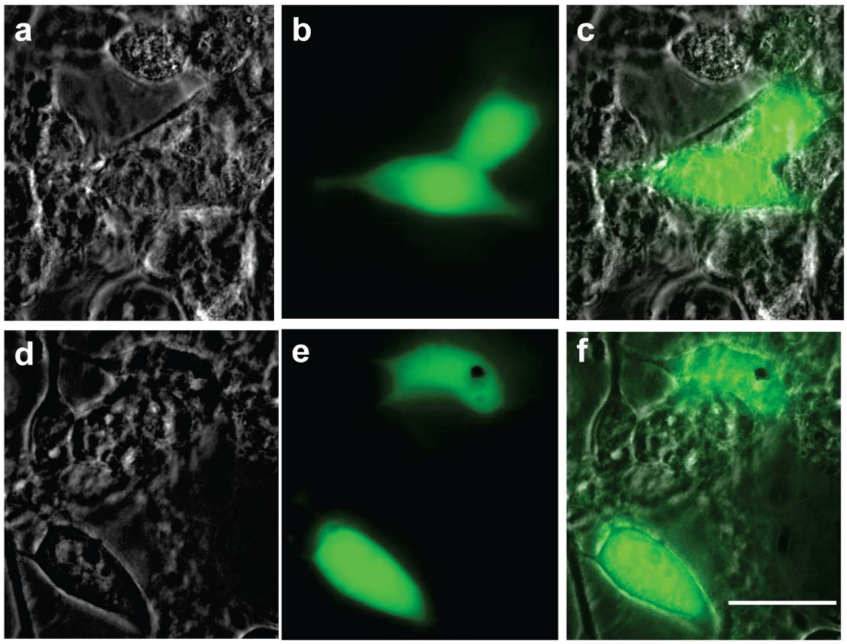

Figure 5 | CMCNP-assisted photothermal delivery (PTD) of ChR2-YFP encoding plasmids into PC3 cells using cw NIR laser beam. (a) Bright field, (b) YFP-fluorescence and (c) composite images of PC3 cells transfected with ChR2-YFP plasmids using PTD. (d–f) Bright field, YFP-fluorescence and composite images of PTD-transfected PC3 cells in another region of interest. Scale bar: 10 μm.

advantages of minimizing the applied concentration and also the laser dose for PTD. The heating induced flow can further help in directing the exogenous material to the sites of delivery as demonstrated in the in-vitro experiments. Therefore, our hybrid-fields based approach can also prove to be very useful for in-vivo applications. While magnetic nanoparticles have recently been used in thermal therapy[49,50], application of AC magnetic field may not be suitable to produce localized hyperthermia as compared to that achievable by the laser beam. Moreover, AC magnetic-field assisted thermal therapy with magnetic nanoparticles require powerful magnetic field[49,51], the safety of which still needs discussion. Though our results show that 720 nm laser beam is more efficient than 800 nm, the variation of % of successful PTD as well as % of damaged cells at 800 nm has a weaker dependence on laser powers over the investigated range. This may indicate that CMCNP-induced PTD using 800 nm is more stable over that using 720 nm and therefore, should be preferred for in-vivo applications. While the reason for such variation is not clear, it is plausible that damage to cells at higher power of 720 nm laser beam may be partly due to direct absorption of cellular components at this wavelength. Since most of the biological samples are better transparent at 800 nm than at 720 nm, it is advantageous to use 800 nm for in-depth PTD.

The CMCNPs, used in the reported experiments, are found to be highly non-reactive due to their crystalline structure, and are very stable in water, as well as physiological solutions, for several months and have very low cytotoxicity, making them an ideal candidate for PTD. Use of MTT assay[47] showed that CMCNPs (concentration up to 25 μg/ml) incubated for as long as 6 hr did not significantly decrease viability of the PC3 cells. These CMCNPs can also be applied in thermal therapy[49,51], drug delivery[52] and even photoacoustic detection of tumor cells[37] due to their controllability under magnetic field. In particular, the strong photothermal absorption of these nanomaterials in NIR demonstrates the possibility of drug delivery or gene transfection into cells in-vivo. The high NIR absorption characteristics of the CMCNPs will allow use of NIR laser beam and thus in-depth delivery in tissue. The penetration depth of the NIR beam can be further enhanced by use of free-space or even fiber-optic Bessel beam[53]. Further, with the intrinsic magnetic property of the CMCNPs, it will be possible to prevent the diffusion of nanoparticles out of the targeted area and thus maintain them in the targeted tissue regions without being washed away by the blood flow. However, since sizes of the CMCNPs are in 5–20 nm range, they can be easily excreted by reticuloendothelial system[54] after in-vivo PTD.

Our previous study demonstrated[55] use of the magnetic-field assisted photothermal destruction of tumor cells using NIR laser beam. For efficient destruction of tumor and further elimination of residual cancer cells in margin of tumor, chemotherapeutic agents can be delivered to tumor cells by the PTD method. Though it is feasible to apply hybrid field (magnetic field for concentrating and light for photothermal effect) in superficial organs and in small animals, difficulties may arise for clinical applications because of the complexities involved in designing a high power focused magnetic field, and the time required to localize therapeutic levels of nanoparticles. Use of a Halbach cylinder[56] can extend the penetration depth of the magnetic field so as to reduce the time required for in-vivo localization. Though the in-vitro experiments showed that PTD into targeted cells is possible using CMCNPs and CW NIR laser beam, in-vivo applications in the targeted tissues needs further evaluation.

Compared with pulsed lasers, CW NIR (diode) lasers are compact, easy-to-use and less expensive, thus the PTD method presented here has significant translational potential. Since the photothermal properties[57] (e.g. thermal conductivity) of crystalline carbon nanostructures are significantly higher (100–2000 W/mK) as compared to amorphous CNPs (0.01–0.1 W/mK), efficiency of photothermal delivery while using different types of MCNPs (graphitic, diamond-like and amorphous) at the same laser parameters (power, exposure and wavelength) is expected to be different. It may be important to evaluate the PTD efficiency at different wavelengths for various types of CMCNPs in order to utilize specific spectral absorption properties of different types of CMCNPs. The strong photothermal absorption of these nanomaterials in NIR open up the possibility of *in vivo* delivering of drugs, proteins (for vaccination) and genes into targeted cells. Besides delivery of naked DNA, the photothermal delivery method can be used for efficient transfer of vaccination proteins. This method, therefore, can also act as a non-invasive, potent, vac-

cine "adjuvant" as compared to existing physical methods (intradermal injection, electroporation and pulsed visible laser irradiation) and chemical or biological agents. By photothermal action, the CMCNPs can also be used for temperature-mediated controllable drug delivery.

Conclusions

Crystalline and magnetic carbon nanoparticles are developed with unique properties as efficient photothermal agents. This enabled replacement of fs laser microbeam with a CW laser beam for photothermal delivery (PTD) of exogenous otherwise impermeable molecules in various cell types. Use of external DC magnetic field and continuous wave (CW) NIR laser beam for magnetic-field assisted, targeted photothermal delivery of opsin-encoding plasmids was successfully demonstrated. Due to significant absorption in the NIR spectrum by CMCNPs, PTD under *in-vivo* condition at large depths is feasible. The results of our study suggest that CMCNP based photothermal poration is a viable approach to remotely guide drug and gene delivery.

Methods

Synthesis of crystalline and magnetic CNPs. The crystalline magnetic carbon nanoparticles (CMCNPs) are synthesized in liquid benzene, using the electric plasma discharge generated between two electrodes in the cavitation field of an ultrasonic horn. The two electrodes were placed ~0.7 mm apart and 1 cm beneath the ultrasonic horn. The ultrasonic horn is set at 600 W and 20 kHz in 100 ml of liquid benzene. After ~1 hour, black carbon powder was produced by dissociation of benzene molecules leading to change in the color of the liquid. The powder is separated by centrifugation from the benzene, dispersed in ethanol and dried in a vacuum oven. During the plasma formation, Fe-electrodes erode and 1–2% of Fe gets embedded into the carbon matrix, making them magnetic.

Estimation of forces on CMCNPs due to external DC magnetic field. A Hall effect gauss meter (421, Lakeshore) was used to measure the magnetic field exerted by the Neodymium Iron Boron magnet. The magnet was fixed and the measurements were recorded at varying distances using the Gauss meter probe. Any external magnetic force exerted on the particle is a translational force directed along the applied field vector and is dependent on the magnetic properties of the particle and the surrounding medium, the size and shape of the particles and the product of the magnetic flux density and the field gradient.

$$\text{According to the equation for magnetic force } F = -\nabla\varphi \tag{1}$$

$$\text{where } \phi = -\mu.B \tag{2}$$

is the scalar potential, μ the relative permeability and B is the magnetic field.

$$\text{Thus, } F = \mu\nabla B \tag{3}$$

$$\text{where } \mu,\ \mu = \mu_0[1+\chi_M] \tag{4}$$

$$\text{and } \chi = M/H \tag{5}$$

where χ is the magnetic susceptibility, M is magnetization and H is magnetic field strength.

Absorption spectroscopic measurement. Absorption measurements were made by a spectrophotometer (Lambda EZ 210, Perkin-Elmer). CMCNP powder was diluted in D_2O. The absorption of the CMCNPs was measured in D_2O in order to avoid water absorption peaks in near-infrared. The CMCNP solution was ultra-sonicated for an hour before absorption measurement. The reference was taken with D_2O solution in a quartz cell of 1 cm path length and absorption spectrum of the well-dispersed sample was measured over NIR wavelength range (700 to 1000 nm). The sample was continuously diluted to a final concentration of 28 μg/ml so as to avoid the scattering tail.

Cell culture and incubation with CMCNPs. Human prostate cancer (PC3) cells and human fibroblast sarcoma (HT1080) cells were routinely cultured in Dulbecco's modified Eagle's medium (DMEM) supplemented with 5% fetal bovine serum (FBS). The cultures were maintained at 37°C in a 5% CO_2 humidified atmosphere. For photothermal treatment, cells were trypsinized, plated on glass coverslip-bottom dishes and used after 24 hours of culturing. CMCNPs were added into culture media to a final concentration of 25 μg/ml and incubated at 37°C in a 5% CO_2 humidified atmosphere for 1–2 hours before PTD experiment. DMEM and FBS were purchased from Lonza (MD, US). Trypsin was purchased from Mediatech (Manassas, USA). All other reagents were purchased from Fisher Scientific except those specifically mentioned.

NIR laser beam irradiation and cellular imaging. A cw Ti: Sapphire laser (Maitai HP, Newport Spectra-Physics Inc) beam in mode lock off condition with a wavelength tuning range from 690 to 1040 nm was directed towards the sample through an inverted optical microscope (Ti-U, Nikon). The exposure time (0 to 20 s) was controlled by a mechanical shutter (S, Uniblitz). A 20× objective (MO, NA = 0.5) was used to focus the laser beam for photothermal irradiation. The dichroic mirror 1 (DC1) combined the laser beam and the beam from the excitation source. The dichroic mirror 2 (DC2) reflects the excitation lamp light and transmits the emitted fluorescence to the CCD. The emission filter (EM) blocked the laser NIR wavelength. Bright field and fluorescence images were captured with exposure of 100 ms using a cooled CCD camera (Coolsnap ES, Photometrics Inc.) and processed using ImageJ Software.

Once magnetic field is applied for few hours to localize the nanoparticles near region of interest, the cells were stained with Calcein (1 μM, Invitrogen) at 37°C for 15 min before experiment. Propidium iodide (PI, 5 μM) was added immediately before laser irradiation under inverted fluorescent microscope (Nikon Ti-U) using the 20× objective. The laser beam power at the sample plane was measured using a power meter (PM100D, Thorlabs). The power of the laser beam was varied (20 to 100 mW) by controlling the angle of orientation of a Glan-Thompson polarizer (P) in the beam path. The XY-scanning of the region of interest (to be irradiated by the laser beam) was achieved by controlling the motorized sample stage movement. Live-dead assay was conducted to determine viability of cells surrounding the irradiation zone. Inclusion of Calcein and exclusion of PI respectively indicates live and dead cell. PI is a membrane impermeable nuclear stain which has characteristics red fluorescence.

1. Luo, D. & Saltzman, W. M. Synthetic DNA delivery systems. *Nat Biotech* **18**, 33–37 (2000).
2. Yu, J.-Y., DeRuiter, S. L. & Turner, D. L. RNA interference by expression of short-interfering RNAs and hairpin RNAs in mammalian cells. *Proc. Nat. Acad. Sci.* **99**, 6047–6052 (2002).
3. Burridge, K. & Feramisco, J. R. Microinjection and localization of a 130 K protein in living fibroblasts: a relationship to actin and fibronectin. *Cell* **19**, 587–595 (1980).
4. Akilov, O. E. *et al.* Vaccination with photodynamic therapy-treated macrophages induces highly suppressive T-regulatory cells. *Photodermatol. Photoimmunol. Photomed.* **27**, 97–107 (2011).
5. Somia, N. & Verma, I. M. Gene therapy: trials and tribulations. *Nat Rev Genet* **1**, 91–99 (2000).
6. Verma, I. M. & Somia, N. Gene therapy - promises, problems and prospects. *Nature* **389**, 239–242 (1997).
7. Tsien, R. Y. The Gree Fluorescent Protein. *Ann. Rev. Biochem.* **67**, 509–544 (1998).
8. Kamimura, K., Suda, T., Zhang, G. & Liu, D. Advances in Gene Delivery Systems. *Pharmaceut. Med.* **25**, 293–306 (2011).
9. Nagel, G. *et al.* Channelrhodopsin-2, a directly light-gated cation-selective membrane channel. *Proc. Nat. Acad. Sci.* **100**, 13940–13945 (2003).
10. Boyden, E. S., Zhang, F., Bamberg, E., Nagel, G. & Deisseroth, K. Millisecond-timescale, genetically targeted optical control of neural activity. *Nat Neurosci* **8**, 1263–1268 (2005).
11. Mohanty, S. K. *et al.* In-Depth Activation of Channelrhodopsin 2-Sensitized Excitable Cells with High Spatial Resolution Using Two-Photon Excitation with a Near-Infrared Laser Microbeam. *Biophys. J.* **95**, 3916–3926 (2008).
12. Zufferey, R., Nagy, D., Mandel, R. J., Naldini, L. & Trono, D. Multiply attenuated lentiviral vector achieves efficient gene delivery in vivo. *Nat Biotech* **15**, 871–875 (1997).
13. Ruitenberg, M. J., Eggers, R., Boer, G. J. & Verhaagen, J. Adeno-associated viral vectors as agents for gene delivery: application in disorders and trauma of the central nervous system. *Methods* **28**, 182–194 (2002).
14. Naldini, L. *et al.* In Vivo Gene Delivery and Stable Transduction of Nondividing Cells by a Lentiviral Vector. *Science* **272**, 263–267 (1996).
15. Thomas, C. E., Ehrhardt, A. & Kay, M. A. Progress and problems with the use of viral vectors for gene therapy. *Nat Rev Genet* **4**, 346–358 (2003).
16. King, R. Gene Delivery to Mammalian Cells by Microinjection. *Methods in Molecular Biology* **245**, 167–173 (2004).
17. Li, S. & Huang, L. Nonviral gene therapy: promises and challenges. *Gene Ther* **7**, 31–34 (2000).
18. Ferber, D. Safer and Virus-Free? *Science* **294**, 1638–1642 (2001).
19. Newman, C. M., Lawrie, A., Brisken, A. F. & Cumberland, D. C. Ultrasound Gene Therapy: On the Road from Concept to Reality. *Echocardiography* **18**, 339–347 (2001).
20. Templeton, N. S. *et al.* Improved DNA: liposome complexes for increased systemic delivery and gene expression. *Nat Biotech* **15**, 647–652 (1997).
21. Panyam, J. & Labhasetwar, V. Biodegradable nanoparticles for drug and gene delivery to cells and tissue. *Adv. Drug Deliv. Rev.* **55**, 329–347 (2003).
22. Tao, W., Wilkinson, J., Stanbridge, E. J. & Berns, M. W. Direct gene transfer into human cultured cells facilitated by laser micropuncture of the cell membrane. *Proc Natl Acad Sci U S A* **84**, 4180–4184 (1987).
23. Schneckenburger, H., Hendinger, A., Sailer, R., Strauss, W. S. & Schmitt, M. Laser-assisted optoporation of single cells. *J Biomed Opt* **7**, 410–416 (2002).

24. Palumbo, G. *et al.* Targeted gene transfer in eucaryotic cells by dye-assisted laser optoporation. *J Photochem Photobiol B* **36**, 41–46 (1996).
25. Mohanty, S. K., Sharma, M. & Gupta, P. K. Laser-assisted microinjection into targeted animal cells. *Biotech. Lett.* **25**, 895–899 (2003).
26. Hosokawa, Y. *et al.* Gene delivery process in a single animal cell after femtosecond laser microinjection. *Appl. Surf. Sci.* **255**, 9880–9884 (2009).
27. Stracke, F., Rieman, I. & König, K. Optical nanoinjection of macromolecules into vital cells. *Journal of Photochemistry and Photobiology B: Biology* **81**, 136–142 (2005).
28. Schinkel, H., Jacobs, P., Schillberg, S. & Wehner, M. Infrared picosecond laser for perforation of single plant cells. *Biotechnol. Bioeng* **99**, 244–248 (2008).
29. Tirlapur, U. K. & Konig, K. Targeted transfection by femtosecond laser. *Nature* **418**, 290–291 (2002).
30. Gu, L. & Mohanty, S. K. Targeted microinjection into cells and retina using optoporation. *J Biomed Opt* **16**, 128003–128006 (2011).
31. Kim, B. *et al.* Tuning payload delivery in tumour cylindroids using gold nanoparticles. *Nat Nano* **5**, 465–472 (2010).
32. Cheng, Y. *et al.* Delivery and efficacy of a cancer drug as a function of the bond to the gold nanoparticle surface. *Langmuir* **26**, 2248–2255 (2010).
33. Petrelli, F., Borgonovo, K. & Barni, S. Targeted delivery for breast cancer therapy: the history of nanoparticle-albumin-bound paclitaxel. *Expert Opin Pharmacother* **11**, 1413–1432 (2010).
34. Huang, X. & El-Sayed, M. A. Gold nanoparticles: Optical properties and implementations in cancer diagnosis and photothermal therapy. *Journal of Advanced Research* **1**, 13–28 (2010).
35. Day, E. S., Morton, J. G. & West, J. L. Nanoparticles for Thermal Cancer Therapy. *Journal of Biomechanical Engineering* **131**, 074001–074005 (2009).
36. Zharov, V. P. *et al.* Photoacoustic flow cytometry: principle and application for real-time detection of circulating single nanoparticles, pathogens, and contrast dyes in vivo. *J Biomed Opt* **12**, 051503 (2007).
37. Galanzha, E. I. *et al.* In vivo magnetic enrichment and multiplex photoacoustic detection of circulating tumour cells. *Nat Nano* **4**, 855–860 (2009).
38. Gannon, C. J. *et al.* Carbon nanotube-enhanced thermal destruction of cancer cells in a noninvasive radiofrequency field. *Cancer* **110**, 2654–2665 (2007).
39. Kostarelos, K., Bianco, A. & Prato, M. Promises, facts and challenges for carbon nanotubes in imaging and therapeutics. *Nat Nano* **4**, 627–633 (2009).
40. De la Zerda, A. *et al.* Carbon nanotubes as photoacoustic molecular imaging agents in living mice. *Nat Nanotechnol* **3**, 557–562 (2008).
41. Wang, S. *et al.* Photothermal Effects of Supramolecularly Assembled Gold Nanoparticles for the Targeted Treatment of Cancer Cells. *Angewandte Chemie* **122**, 3865–3869 (2010).
42. Tong, L. *et al.* Gold Nanorods Mediate Tumor Cell Death by Compromising Membrane Integrity. *Advanced Materials* **19**, 3136–3141 (2007).
43. Huang, X., El-Sayed, I. H., Qian, W. & El-Sayed, M. A. Cancer Cell Imaging and Photothermal Therapy in the Near-Infrared Region by Using Gold Nanorods. *Journal of the American Chemical Society* **128**, 2115–2120 (2006).
44. Gobin, A. M. *et al.* Near-Infrared Resonant Nanoshells for Combined Optical Imaging and Photothermal Cancer Therapy. *Nano Letters* **7**, 1929–1934 (2007).
45. Brongersma, M. L. Nanoscale photonics: Nanoshells: gifts in a gold wrapper. *Nat Mater* **2**, 296–297 (2003).
46. Chen, J. *et al.* Immuno Gold Nanocages with Tailored Optical Properties for Targeted Photothermal Destruction of Cancer Cells. *Nano Letters* **7**, 1318–1322 (2007).
47. Gu, L., Vardarajan, V., Koymen, A. R. & Mohanty, S. K. Magnetic-field-assisted photothermal therapy of cancer cells using Fe-doped carbon nanoparticles. *J Biomed Opt* **17** (2012).
48. Wang, B.-G., Riemann, I., Schubert, H., Halbhuber, K.-J. & Koenig, K. In-vivo intratissue ablation by nanojoule near-infrared femtosecond laser pulses. *Cell and Tissue Research* **328**, 515–520 (2007).
49. Ito, A. *et al.* Tumor regression by combined immunotherapy and hyperthermia using magnetic nanoparticles in an experimental subcutaneous murine melanoma. *Cancer Sci* **94**, 308–313 (2003).
50. Fan, X. *et al.* [Preparation and characterization of magnetic nano-particles with radiofrequency-induced hyperthermia for cancer treatment]. *Sheng Wu Yi Xue Gong Cheng Xue Za Zhi* **23**, 809–813 (2006).
51. Jordan, A. *et al.* The effect of thermotherapy using magnetic nanoparticles on rat malignant glioma. *Journal of Neuro-Oncology* **78**, 7–14 (2006).
52. Salloum, M., Ma, R. H., Weeks, D. & Zhu, L. Controlling nanoparticle delivery in magnetic nanoparticle hyperthermia for cancer treatment: experimental study in agarose gel. *Int J Hyperthermia* **24**, 337–345 (2008).
53. Mohanty, S. K., Mohanty, K. S. & Berns, M. W. Manipulation of mammalian cells using a single-fiber optical microbeam. *J Biomed Opt* **13** (2008).
54. Faraji, A. H. & Wipf, P. Nanoparticles in cellular drug delivery. *Bioorg Med Chem* **17**, 2950–2962 (2009).
55. Gu, L., Vardarajan, V., Koymen, A. R. & Mohanty, S. K. Magnetic-field-assisted photothermal therapy of cancer cells using Fe-doped carbon nanoparticles. *J. Biomed. Opt.* **17**, 018003–018009 (2012).
56. Riegler, J. *et al.* Magnetic cell delivery for peripheral arterial disease: A theoretical framework. *Med Phys* **38**, 3932–3943 (2011).
57. Balandin, A. A. Thermal properties of graphene and nanostructured carbon materials. *Nat Mater* **10**, 569–581 (2011).

Acknowledgments

The authors would like to thank Sunil Gaussian for help in preparation of the sample and its characterization and Alex Villalobos for help during preliminary experiments. SM would like to thank the support from the National Institute of Health (NS084311) and National Science Foundation (1148541) and Office of President and Provost, The University of Texas at Arlington.

Author contributions

S.M. and A.K. designed and supervised the project. A.K. and S.M. characterized the nanoparticles. L.G. and S.M. performed the poration experiments. L.G., A.K. and S.M. analyzed the data and wrote the paper.

Additional information

Supplementary information accompanies this paper at http://www.nature.com/scientificreports

Competing financial interests: The authors declare no competing financial interests.

How to cite this article: Gu, L., Koymen, A.R. & Mohanty, S.K. Crystalline magnetic carbon nanoparticle assisted photothermal delivery into cells using CW near-infrared laser beam. *Sci. Rep.* **4**, 5106; DOI:10.1038/srep05106 (2014).